Scientific Paper

Submitted date: 05/12/18

IABSE Task Group 3.1 benchmark results. Part 1: numerical 2-degree-of-freedom sectional deck model with analytical aerodynamics

Giorgio Diana, *Chair of Task Group 3.1, Politecnico di Milano, Italy*

Stoyan Stoyanoff, *Vice-chair of Task Group 3.1, RWDI, Canada*

Ketil Aas-Jakobsen, *Dr. Ing. A. Aas-Jakobsen AS, Norway*

Andrew Allsop, *ARUP, United-Kingdom*

Michael Andersen, *Svend Ole Hansen ApS, Denmark*

Tommaso Argentini, *Politecnico di Milano, Italy*

Miguel Cid Montoya *University of A Coruna, Spain*

Santiago Hernández *University of A Coruna, Spain*

José Ángel Jurado *University of A Coruna, Spain*

Hiroshi Katsuchi *Yokohama National University, Japan*

Igor Kavrakov *Bauhaus-University Weimar, Germany*

Ho-Kyung Kim *Seoul National University, Korea*

Guy Larose *RWDI, Canada*

Allan Larsen *COWI, Denmark*

Ole Øiseth *Norwegian University of Science and Technology, Norway*

Simone Omarini *Politecnico di Milano, Italy*

Daniele Rocchi *Politecnico di Milano, Italy*

Martin Svendsen *Ramboll, Denmark*

Teng Wu *University of Buffalo, USA*

Contact: tommaso.argentini@polimi.it

Abstract

IABSE Task Group 3.1 has mandate to define reference results for the validation of methodologies and programs used to study both stability and buffeting response of long-span bridges. These tools for the simulation of the aeroelastic behaviour are indeed fundamental in the safe design of bridges and they should be validated.

The workgroup decided to setup a benchmark procedure consisting of several steps to define reference results for this validation. For each step, contributors use their own methodology to simulate the bridge behaviour using the same input data. All the results are then compared, and reference values are defined through a statistical analysis. The benchmark procedure is thought as a 3-step problem with sub-steps of increasing difficulty: Step 1 compares numerical results only, Step 2 is a validation against wind tunnel experiments, and Step 3 against full-scale data.

In this paper, the contributions and the reference results of the simplest initial sub-step (1.1.a) are presented. It consists in the simulation of the aeroelastic response of a 2-degree of freedom sectional model, with analytical aerodynamic coefficients, forced by turbulent wind. Despite the problem simplicity, differences in some contributions are significant, confirming the necessity of having solid references to validate software programs.

Keywords: benchmark; aeroelasticity; flutter; buffeting; long-span bridge; validation

1 Introduction

1.1 Task Group 3.1: super-long span bridge aerodynamics

The assessment of the dynamic response of long-span bridges to turbulent wind is one of the major challenges for designers, since excessive wind-induced vibrations may lead to comfort, fatigue and structural strength problems. Moreover, structural safety verifications must account for the bridge aeroelastic instabilities.

Methodologies and software programs used for the assessment of the aeroelastic behaviour of long span bridges should be validated against benchmark results. In other engineering fields, procedures to certify software programs are available; as an example, we can list the following:

a) software programs for computing the response of High Voltage Transmission lines to vortex induced vibrations and sub-span oscillations are validated through benchmarks between different programs and against field measurements, as presented in Refs. [1].
b) the European Standard defines the procedure to validate the software programs for computing train dynamics to support homologation, through comparison between analytical and experimental results, as proposed in Refs. [2] [3]
c) A European Standard is available to certify the software programs for computing pantograph-catenary interaction using a reference result, as presented in Refs. [4].

For bridge aeroelasticity, on the contrary, up to now, there are not well-established or standardized procedures for validation of numerical methodology and software programs adopted for stability and buffeting response analyses of super-long span bridges. Therefore, the IABSE Task Group 3.1 (extended name: “super-long span bridge aerodynamics”) was promoted to propose a validation procedure based on the state of the art in this field.

To define reference results for comparison in this validation, the Task Group (TG) decided to set up a benchmark procedure that consists of multiple steps with increasing level of complexity. For each step, TG members use their own methodology and codes to simulate the bridge behaviour, with the same input data. All the results are then compared, and reference values are defined with a statistical analysis. They are finally published for everyone who wants to validate their methodologies and numerical codes.

Currently, TG 3.1 members are academic researchers, consultants and designers with great experience of bridge studies and design, affiliated to Aas-Jakobsen, ARUP, Bauhaus University, Bentley Systems, Bouygues Construction, COWI, Greisch, Norwegian University of Science and Technology, Parsons, Politecnico di Milano, Ramboll, RWDI, Seoul National University, Svend Ole Hansen ApS, Tonji University, University of A Coruna, University of Buffalo, University Southern Denmark, and Yokohama National University. Each research group has his own methodology to solve the bridge response to wind, either in time domain (TD) or in frequency domain (FD) and the description of their the methodologies employed in the current paper can be found in the proposed Refs. [5] [6] [7] [8] [9] [10] [11] [12] [13] [14] [15] [16] [17] [18] [19] [20] [21] [22] [23] [24] [25] [26] [27].

1.2 TG3.1 Benchmark structure

TG3.1 benchmark consists of 3 principal steps (Step 1, 2, and 3) with sub-steps of increasing complexity. For each Step, same input data are used and shared among all the participants. The results, obtained through the different methodologies adopted by the TG participants, will be analyzed to define reference values to validate the software programs, as it will be explained in Section 3.

1.2.1 Step 1

Step 1 is a comparison of results obtained from different numerical algorithms developed to analyse the stability and the buffeting response of a bridge. This Step has 2 sub-steps with increasing level of complexity:

- Step 1.1 that considers a deck sectional model;
- Step 1.2 that analyses a full bridge model.

In their turn, both Step 1.1 and Step 1.2 have their sub-steps:

a) Step 1.1a is the simplest case. It is the topic of this paper and it is fully discussed in the next sections. This case examines the stability and the buffeting response of a deck sectional model with 2 degree-of-freedom (DOF): vertical and torsional. The analytical Theodorsen functions of a flat plate are used to define aerodynamic forces as analytical functions of the reduced velocity. Only the vertical component *w* of wind turbulence is considered, with an analytical formulation to compute buffeting forces.

b) Step 1.1c introduces some complexities with respect to 1.1a: experimental aerodynamic coefficients, defined in a limited range of reduced velocities, and 3 degree-of-freedom (vertical, torsional, and lateral). Moreover, both the vertical and the horizontal components of turbulence, *w* and *u,* are considered.

c) Step 1.2a studies the stability and the buffeting response of a full bridge forced by a turbulent wind field, where the horizontal and vertical components change in time and space (along the bridge axis). The Storebælt bridge structure is considered, using a modal approach with the first 12 vibration modes. Experimental aerodynamic coefficients at 0-degree angle of attack are used to simplify the analysis.

d) Step 1.2b introduces additional complexity with respect to 1.2a: experimental aerodynamic coefficients dependency upon the angle on attack is considered.

Step 1.1c has been already completed, and the results will be published as Part 2 of this article. Step 1.2 is on going and an extended paper with its results will be issued in 2019.

1.2.2 Step 2

Step 2 will be a comparison of predicted numerical results and wind tunnel experimental tests. The experimental tests have been already performed on a 2 degree-of-freedom sectional model of the Yavuz Sultan Selim Bridge (Third Bosphorus Bridge).

The complete set of aerodynamic coefficients were measured on this sectional model: drag, lift and moment static coefficients, flutter derivatives and admittance functions as functions of the mean angle of attack.

Aeroelastic tests were performed on the model suspended on springs. Frequencies, damping ratios and modes of vibration were measured at different mean wind speeds to assess aeroelastic stability.

Buffeting tests were performed using an active turbulence generator available at the wind tunnel of Politecnico di Milano (POLIMI), see Refs. [26].

The results of the experimental campaign have already been distributed to all TG members and results collection is on going.

1.2.3 Step 3

Step 3 will be a comparison of numerical results against full scale measurements on a real bridge, if available in the future. Monitoring data will be used for a benchmark case at full scale in which all the input and output data of the bridge will be available for all the participants.

1.2.4 Benchmark input data

In the Supplemental Material of each TG paper dealing with a specific step, the corresponding input data are provided. As an alternative, the same data can be downloaded from the IABSE website.

Everyone can check their numerical codes using these data.

2 Benchmark: Step 1.1a

As introduced in the previous section, Step 1.1a studies a 2-DOFs (vertical and torsional) deck sectional model with analytical aerodynamic coefficients.

Input data were provided to all TG contributors, and they are described in Section 2.1, while the output results are compared in Section 3 and they are described in Section 2.2.

2.1 Input for Step 1.1a analysis

The input data for the simulation of the deck response are the following:

- structural parameters of the deck sectional model
- turbulent wind characteristics
- aerodynamic coefficients

2.1.1 Structural parameters

Structural input data of the sectional model are reported in Table 1. The real full-scale values (mass per unit length, structural natural frequencies, damping ratio and deck chord) of the Storebælt bridge are used. Only the parameters of first vertical and torsional modes of the full bridge are considered for the sectional model.

Table 1. Sectional model structural data

Quantity	Description	Value
m_L [kg/m]	Mass per unit length	22740
J_L [kgm^2/m]	Moment of Inertia per unit length	2.47×10^6
B [m]	Deck chord	31
f_z [Hz]	Vertical structural frequency	0.10
f_θ [Hz]	Torsional structural frequency	0.278
ξ [-]	Damping ratio (for both modes)	0.003

2.1.2 Turbulent wind characteristics

The mean wind speed U and only the vertical component of turbulent wind are considered, since only the vertical and torsional motion are investigated. Five mean wind speed scenarios are considered to compare results with an increasing level of aerodynamic coupling up to a wind speed close to flutter instability. The characteristics of the

simulated wind are reported in Table 2. Ten 600-second long time histories of the vertical wind component were generated through the Von Karman spectrum reported in Table 2, to allow the use of time-domain methods. A harmonic superposition method is used for the generation of the time histories (see Refs. [28] [29]). The time histories of $w(t)$ are available in the Supplemental Material.

The method used for the wind generation was selected for convenience: the investigation of the wind field generation problem is not a task of the benchmark and it is beyond the scope of this study.

Table 2. Incoming wind characteristics

Wind speeds	U = 15, 30, 45, 60, 75 m/s
Air density	$\rho = 1.22 \text{kg/m}^3$
Turbulence intensity	$I_w = \frac{\sigma_w}{U} = 0.05$
Integral length scale	${}^{x}L_w$ = 20 m
Von Karman power spectrum of w	$\frac{f \cdot S_w(f)}{{\sigma_w}^2} = \frac{4\left(\frac{f\ {}^{x}L_w}{U}\right)}{\left[1+283.2\left(\frac{f\ {}^{x}L_w}{U}\right)^2\right]^{11/6}}\left(1+755.2\left(\frac{f\ {}^{x}L_w}{U}\right)\right.$

2.1.3 Aerodynamic forces

The standard approach to write the aerodynamic forces is based on a linearized model of the fluid-structure interaction around a steady configuration of the bridge, which depends on the mean wind speed.

The aerodynamic forces (F_{aero}) acting on the deck can be modelled as the sum of three different components, namely:

- F_{ST} ,the stationary aerodynamic forces
- F_{se}, the self-excited (or motion-induced) forces
- F_{buff}, the buffeting forces.

The stationary aerodynamic forces F_{ST} depend on the mean wind speed only, the self-excited forces F_{se} depend on bridge motion, and the buffeting forces F_{buff} depend on the incoming wind turbulence.

According to the sign conventions reported in Figure 1, the steady aerodynamic drag, lift and moment acting on the deck section of unitary length are defined through steady coefficients as functions of the angle of attack α:

$$F_{ST} = \frac{1}{2}\rho U^2 B \begin{bmatrix} C_D(\alpha) \\ C_L(\alpha) \\ B\ C_M(\alpha) \end{bmatrix} \quad (1)$$

where B is the deck chord, U the mean wind velocity, and ρ the air density. C_D, C_L, C_M are respectively the drag, lift and moment static coefficients, usually measured through wind tunnel tests.

For Step 1.1a, the aerodynamics of a flat plat is considered, around zero angle of attack. Therefore, $C_D = 0$, while the static lift and moment aerodynamic coefficients are defined as:

$$\begin{bmatrix} C_L \\ C_M \end{bmatrix} = \begin{bmatrix} K_L \\ K_M \end{bmatrix} \alpha = \begin{bmatrix} 0 \\ 0 \end{bmatrix} \quad (2)$$

where $K_L = 2\pi$ and $K_M = \pi/2$ are the first derivative of lift and moment static coefficients with respect to the angle of attack. $\alpha = 0$ since it is equal to the static rotation of the deck $\theta_{st} = 0$. (see Figure 1).

Consequently, the main aim of the benchmark is to compare the dynamic response of the bridge due to the self-excited F_{se} and buffeting forces F_{buff} around the steady configuration of the bridge, in this case always equal to zero ($z_{st} = 0$, $\theta_{st} = 0$).

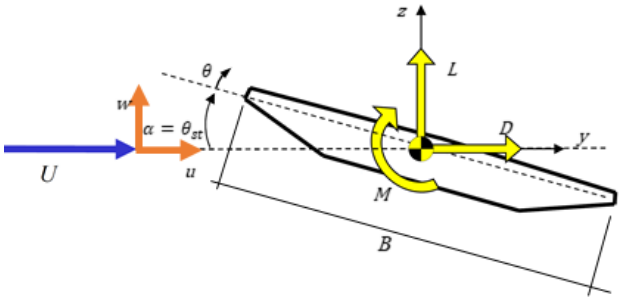

Figure 1. Sign conventions

Self-excited forces F_{se} per unit length are defined through the flutter derivatives coefficients using a linearized approach around the steady position of the bridge. Typically, flutter derivatives coefficients are measured experimentally on rigid sectional models in wind tunnels for a discrete number of reduced velocities requiring an interpolation and/or extrapolation to simulate conditions where experimental data are not available, see Refs [30].

For Step 1.1a the flat plate flutter derivatives values are defined analytically from the Theodorsen function. This choice is due to the will to start with a completely defined problem where the dependence of flutter derivatives on reduced velocity is analytically defined.

The POLIMI formulation for flutter derivatives (see Refs [25]) is used in this paper for convenience, since this notation is closer to the Theodorsen functions. The coefficients in the classical Scanlan formulae are available in the Supplemental Material. Considering a vertical and a torsional harmonic motion around the steady position of the bridge at 0 degree, the self-excited forces per unit length F_{se} acting on the bridge deck are expressed through eight flutter derivatives as:

$$L_{se} = \frac{1}{2}\rho U^2 B \begin{pmatrix} -h_1^* \frac{\dot{z}}{U} - h_2^* \frac{B\dot{\theta}}{U} + h_3^* \theta + \cdots \\ \frac{2\pi^3}{V^{*2}} h_4^* \frac{z}{B} \end{pmatrix} \quad (3)$$

$$M_{se} = \frac{1}{2}\rho U^2 B^2 \begin{pmatrix} -a_1^* \frac{\dot{z}}{U} - a_2^* \frac{B\dot{\theta}}{U} + a_3^* \theta + \cdots \\ \frac{2\pi^3}{V^{*2}} a_4^* \frac{z}{B} \end{pmatrix} \quad (4)$$

where h_i^* are the flutter derivatives for lift force L_{se} and a_i^* are the flutter derivatives for the moment M_{se}; $V^* = U/(fB)$ is the reduced velocity, being f the frequency and B the deck chord; z and θ are respectively the vertical (positive upward) and the torsional (positive nose-up) displacements of the sectional bridge around the static configuration, see Figure 1.

The flutter derivatives defined analytically for a flat plate are (see Refs. [31]):

$$\begin{aligned} h_1^* &= 2\pi F(f^*) \\ h_2^* &= -2\pi\left(\frac{1}{4} + \frac{F(f^*)}{4} + \frac{1}{2\pi} V^* G(f^*)\right) \\ h_3^* &= 2\pi\left(F(f^*) - \frac{\pi}{2V^*} G(f^*)\right) \\ h_4^* &= \left(1 + \frac{2}{\pi} V^* G(f^*)\right) \end{aligned} \quad (5)$$

$$\begin{aligned} a_1^* &= \frac{\pi}{2} F(f^*) \\ a_2^* &= \frac{\pi}{2}\left(\frac{1}{4} - \frac{F(f^*)}{4} - \frac{1}{2\pi} V^* G(f^*)\right) \\ a_3^* &= \frac{\pi}{2}\left(F(f^*) - \frac{\pi}{2V^*} G(f^*)\right) \\ a_4^* &= \frac{V^*}{2\pi} G(f^*) \end{aligned} \quad (6)$$

Where $F(f^*)$ and $G(f^*)$ are the real and imaginary parts of the circulatory Theodorsen function, defined through the Bessel functions J_i and Y_i of the first and second kind ($i = 0, 1$) available in standard computational codes:

$$F(f^*) = \frac{J_1(J_1+Y_0)+Y_1(Y_1-J_0)}{(J_1+Y_0)^2+(Y_1-J_0)^2} \quad (7)$$

$$G(f^*) = -\frac{J_1 J_0 + Y_1 Y_0}{(J_1+Y_0)^2+(Y_1-J_0)^2} \quad (8)$$

Typically, flutter derivatives coefficients are function not only of the reduced velocity V^*, but also of the mean angle of attack, around which the harmonic motion occurs. For Step 1.1a, only zero angle of attack is considered, therefore no contribution due to the aeroelastic drag D_{se} is present and the flutter derivatives of the horizontal motion y are neglected.

The buffeting forces F_{buff} per unit length due to incoming turbulent wind w are defined in frequency domain through the admittance functions

$$\begin{Bmatrix} L_{buff} \\ M_{buff} \end{Bmatrix} = \frac{1}{2}\rho U B \begin{bmatrix} \chi^*_{Lw} \\ B\chi^*_{Mw} \end{bmatrix} \{W_w(f)\} \quad (9)$$

where $W_w(f)$ is the Fourier transform $w(t)$, positive upwards; χ^* are called admittance functions and they depend upon the reduced velocity V^* and the mean angle of attack.

The along wind component (horizontal component) u is not considered for buffeting forces.

Typically, the admittance functions χ^* are measured as a function of the reduced velocity and the mean angle of attack through wind tunnel test on sectional models, in a similar way of what is done for the flutter derivatives coefficients.

In this case, the $\chi^*(V^*)$ are defined using the quasi-steady values weighted by a function $A(V^*)$ as:

$$\chi^*_{Lw} = (K_L + C_D)A(V^*) \quad (10)$$

$$\chi^*_{Mw} = K_M A(V^*) \quad (11)$$

$A(V^*)$ is a real weighing function in reduced velocity. In Step 1.1a, the analytical Davenport formula is used:

$$A(V^*) = \frac{2}{(7/V^*)^2}\left(7/V^* - 1 + e^{-7/V^*}\right) \quad (12)$$

This choice is done again to have a function defined analytically over the complete range of V*.

2.2 Required output for Step1.1a

The following results were provided by the TG members:

1. Aeroelastic stability in smooth flow:
   a. Critical flutter speed of the bridge;
   b. frequency and damping ratio of the two vibration modes as functions of mean wind speed.
2. Buffeting response in turbulent flow:
   a. standard deviation of displacements z and θ as function of mean wind speed;
   b. comparison of power spectra densities (PSD) of z and θ.

These results are presented and analyzed in the following Section, with the aim to select the most meaningful quantities for validating numerical models and corresponding reference values.

3 Results of Step 1.1a

3.1 Aerodynamic stability in smooth flow

Figure 2 shows a plot of the critical flutter speeds computed by the different methods and software programs provided by TG members. Each contribution is reported anonymously by a progressive number. Fourteen contributions have been collected and analysed to define the reference values and a spread band around them.

As expected, all the results are confined in a very narrow range of values (1.5 m/s) since the problem is simple, and input data are defined analytically and shared.

Nevertheless, some contributions seem to be more different from the others and will be considered outliers. A specific procedure is applied to eliminate them and to use the remaining set of results to define the reference values.

TG 3.1 decided to apply the following strategy. If we considered all the contributions, the reference value would be defined as the average value of all the results μ^*, since there is no motivation to prefer one contribution instead of another one. Following this approach, the average value and the spread band plus/minus one standard deviation σ^* are plotted as red lines (red dash-dot line and red dashed-line, respectively), on the results in Figure 2.

Results within this spread band are considered reliable, and outliers are eliminated. As an example, in Figure 2 Contr. 2 and 11 fall out of the spread band, and their effect will be eliminated.

A new reference mean μ and a new standard deviation σ are computed excluding the outlier data and taken as reference: results within $\mu \pm \sigma$ are considered valid.

Reference values are shown in Figure 2, with a dashed black line for μ and a dotted black line for $\mu \pm \sigma$. The reference flutter speed for Step 1.1a is therefore defined as μ = 77.45 m/s and σ = 0.092 m/s, according to this methodology. The two contributions (Contrib. 12 and 13), falling out of the black new spread band, are considered not validated.

The comparison among the natural frequency and the damping ratio of the unstable torsional mode of the bridge deck as functions of the mean wind speed are reported in Figure 3 and Figure 4 respectively.

Looking at the frequency trend (Figure 3), a good agreement among results is present. Only at wind speed values close to flutter speed, some contributions show discrepancies. Contribution 10

is far away from the others at flutter speed in Figure 3, even if it is within the black spread band in Figure 2, and therefore it predicts the flutter critical wind speed in a proper way. On the contrary, looking at Contribution 12, that is out of the black spread band in flutter speed, it is also out from the frequency trend at the flutter speed.

If we look to the damping ratio trend (Figure 4), Contribution 14 is clearly different from the others in all the range of wind speed apart from the region close to the critical flutter speed, when damping ratio crosses the x-axis becoming negative. This means that this method is able to predict the flutter speed close to the reference (see Contribution 14 in Figure 2) but with a wrong aerodynamic coupling in most of the wind speed range.

Excluding Contr.14, most of the discrepancies among the remaining contributions occur after 45 m/s close to the peak of the damping trend of the unstable mode. This shows how different numerical models simulate aeroelastic effects in a different way, also for this very simple and basic case.

In Figure 4 Contribution 10 is different from the others and very close to Contribution 12, already out of the black spread band in Figure 2, and therefore not valid. Contribution 7 shows larger damping than the others in the peak of the damping trend, despite most of the contributions are confined in a very narrow range of values.

These evidences highlight that considering only flutter speed, it is not sufficient to validate numerical codes, and also the damping ratio trends versus the mean wind speed have to be compared with reference data.

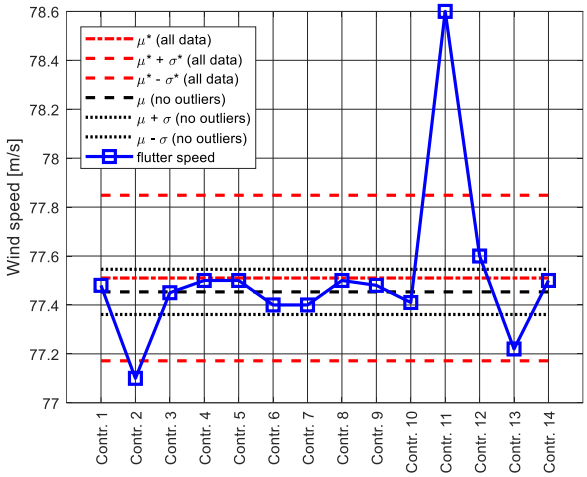

Figure 2. Flutter critical wind speed results from different programs of the TG. Red lines: statistical values using all data; Black lines: statistical values excluding outlier data

Since the eigenvalues/eigenvectors analysis is a numerical iterative routine, there is no analytical method for calculating the trends of frequency and damping ratio. Reference values can only be defined through a statistical analysis of the results.

As done before with the flutter speed, a similar procedure is applied to eliminate outliers in frequency and damping trends. The reference average values are reported in Figure 3-Figure 4, as black crosses. Only the reference μ is reported in the figure as black markers, while the ratio between σ and μ is listed in Table 3 and in Table 4 in Section 4. In these Tables the vertical frequency and damping ratio of the vertical mode are also considered.

The largest σ/μ value is close to the flutter critical wind speed, mainly on the vertical mode, when aeroelastic effects become stronger. In any case, excluding the outliers it is evident that majority of the results are quite similar before 45 m/s, where the aeroelasticity effects are not so large.

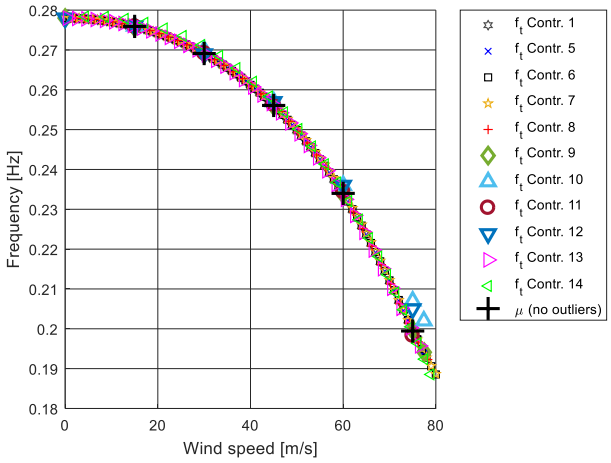

Figure 3. Frequency of the unstable mode as function of mean wind speed

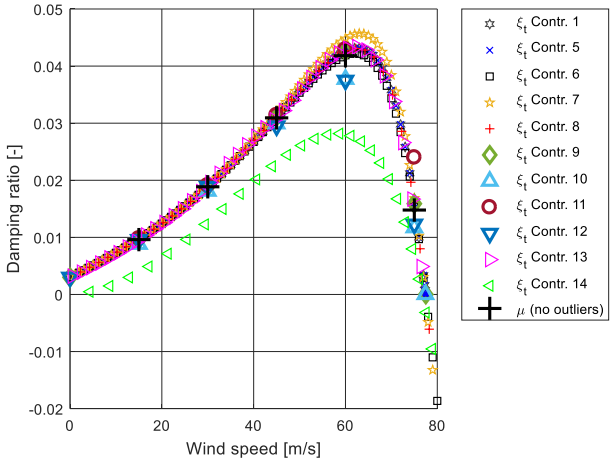

Figure 4. Damping ratio of the unstable mode as function of mean wind speed

TG members emphasize that the flutter speed is not enough to validate numerical codes, and this information must be joined with eigenvalues analysis in order to check the aerodynamic coupling as a function of the mean wind speed.

3.2 Buffeting response in turbulent flow

Comparisons among the root mean square (RMS) values of the vertical (z) and torsional displacement (θ) versus the wind mean speed are presented respectively in Figure 5 and Figure 6. Buffeting response is computed by the TG 3.1 members using time domain (TD) (11 contributions collected) and frequency domain (FD) approaches (10 contributions collected). Torsional values are expressed as equivalent displacement of the deck leading edge according to: $z_{eq} = \frac{B}{2}\theta$. TD results are the average of the ten RMS values of the simulations performed using the provided ten time histories of wind speed.

In Figure 5 and Figure 6 TD and FD results are presented together, but for a better understanding of the plots, frequency domain values are shifted by +1m/s on the x-axis to prevent overlapping.

Figure 5 and Figure 6 report also the statistical analysis of the results excluding outlier data, already described in the previous Section 3.1. The average value μ is plotted with a solid black line, while the curves $\mu \pm \sigma$ are plotted with dashed black lines. In Section 4, Table 5 displays the reference mean μ and the standard deviation ratio σ/μ computed excluding the outlier data at the five tested velocities.

Figure 7 and Figure 8 report the power spectral density (PSD) computed both in frequency and time domain of vertical (z) and torsional equivalent displacement (z_{eq}) for a wind speed of 60 m/s. Only ten contributions in total are available, five in frequency domain and five in time domain. In both the vertical and the equivalent torsional displacement three contributions are very far from the others. RMS values (RMS_z and RMS_{zeq}) computed by integration of the PSDs are reported in the legend, to be compared with Figure 5 and Figure 6.

Considering that in Step 1.1a input data are analytically defined (flat plate aerodynamics from the Theodorsen functions), the different approaches should lead to the same results at least in frequency domain. In this case, instead of defining the statistical reference curve as the average of the collected results, an analytical reference curve is directly computed as reported in Appendix together with a numerical example of PSD computation in FD, at 45 m/s.

The analytical reference power spectra are also used to compute analytical reference RMS to be compared with the statistical average of the available results computed by the TG participants. The analytical RMS computed integrating the power spectra are plotted in Figure 5 and in Figure 6 as gray bars.

The analytical reference values above defined are very close to the statistical ones, confirming that

the procedure used in this paper to define the reference values, when analytical solutions are not available, is reliable thanks to the large number and quality of most of the contributions.

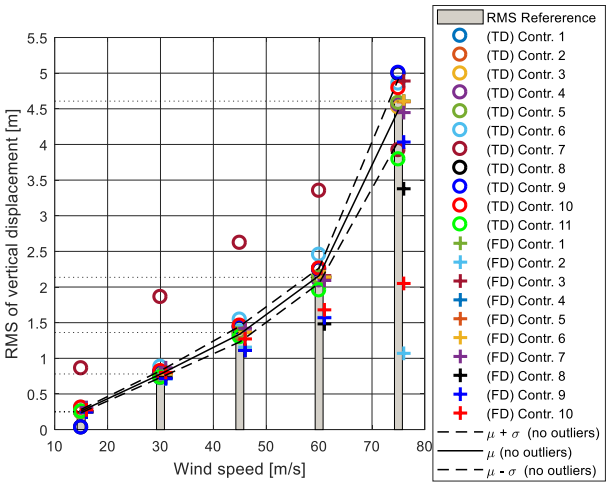

Figure 5. RMS of vertical displacement versus mean wind speed. Black lines: statistical values excluding outlier data

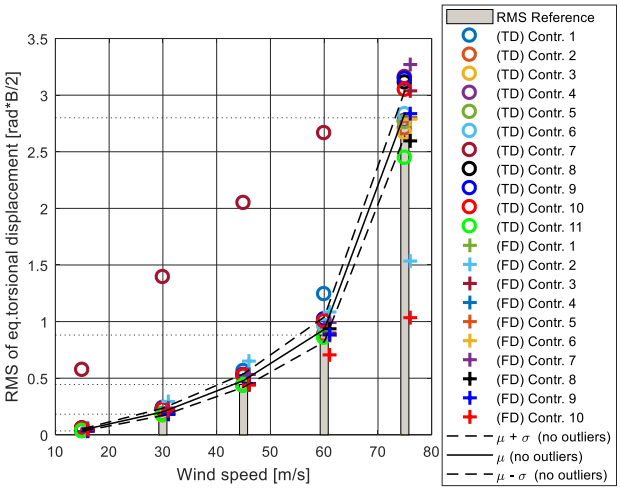

Figure 6. RMS of equivalent torsional displacement versus mean wind speed. Black lines: statistical values excluding outlier data

In Figure 5 and Figure 6 it is clearly visible how data spread increases by increasing wind speed, both for FD and TD approaches, neglecting Contribution 7 (TD), that is an outlier. This effect could be due to the growing aeroelastic coupling between modes at large wind speed. TD and FD approaches show similar values in the torsional equivalent displacement, if we do not consider contributions FD 2, FD 10 and TD 7. This is not the same in the vertical displacement. Considering 60 m/s and 75 m/s, FD approaches show a larger spread compared to TD approaches and they have the lowest values. Even excluding the outliers from the statistics, standard deviation on the vertical displacement reaches 10% at 75 m/s and 7% on the torsional displacement.

Comparing Figure 5 and Figure 7, it is visible that Contribution FD 10, completely different from the other vertical RMS results, has also a complete different shape in the PSD of the vertical displacement, describing only one peak at 0.1 Hz. This evidence highlights how RMS results alone are not sufficient to validate numerical codes. Also the PSD trend versus the frequency has to be compared with reference data, because similar RMS values may have a complete different trends in the PSD. Contribution FD 10, for example, does not consider the aerodynamic coupling in a proper way at 60 m/s and probably in most range of wind speeds. Nevertheless, this is visible only matching the PSD curve with the RMS value. We can not say something similar about Contribution FD 2, since we do not have the PDS results, but probably it describes a wrong aerodynamic coupling near the flutter speed at 75 m/s.

TG members emphasize that there is a big scatter in the results increasing the wind speed and it is already large at a typical design wind speed (e.g. 45 m/s). A smaller spread band around the average is desirable.

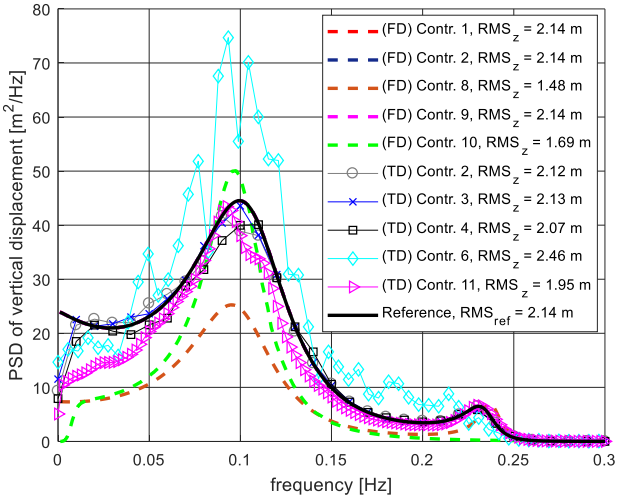

Figure 7. PSD of vertical displacement, 60 m/s wind mean speed

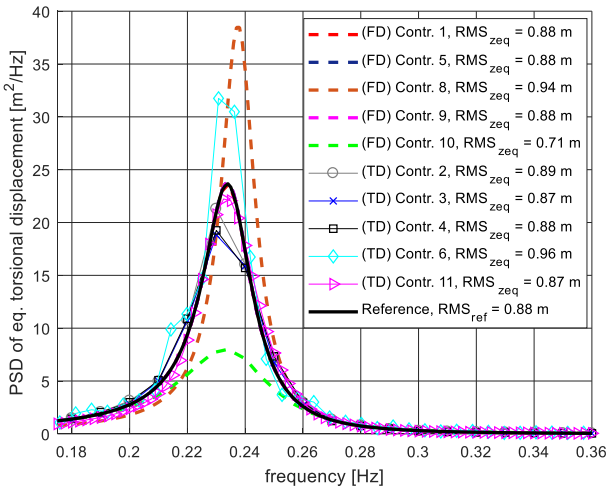

Figure 8. PSD of equivalent torsional displacement, 60 m/s wind mean speed

4 Step 1.1a: reference values

This Section summarizes the reference values presented in the previous sections.

In Table 3, reference values of the natural frequencies of the system as function of the mean wind speed are shown, while in Table 4 the reference values of the damping ratios are shown. Results of the vertical mode (z) and of the torsional mode (θ) are reported at the five tested velocities as reference mean μ and ratio between the standard deviation $\sigma$and μ.

Reference (RMS) values of the buffeting response for the vertical (z) and the equivalent torsional (z_{eq})displacements versus the wind mean speed for Step 1.1a are reported in Table 5. RMS values here reported are defined by the statistical average μ and by normalized standard deviation $\frac{\sigma}{\mu}$ of the different contributions both in TD and FD.

Table 6 and 7 report the reference power spectra S_z and S_θ defined in the previous Section 3.2, for the validation of numerical codes. Five frequencies are selected, and all the five wind velocities are considered.

Table 3. Step 1.1a vertical and torsional frequencies: mean and standard deviation

		15 m/s	30 m/s	45 m/s	60 m/s	75 m/s
f_z [Hz]	μ	0.0987	0.0999	0.1014	0.1027	0.0829
	$\frac{\sigma}{\mu}$	5%	0%	0%	1%	26%
f_θ [Hz]	μ	0.2759	0.2691	0.2561	0.2340	0.1994
	$\frac{\sigma}{\mu}$	0%	0%	0%	0%	0%

Table 4. Step 1.1a vertical and torsional damping ratios: mean and standard deviation

		15 m/s	30 m/s	45 m/s	60 m/s	75 m/s
ξ_z [-]	μ	0.0399	0.0921	0.1689	0.3034	0.5349
	$\frac{\sigma}{\mu}$	1%	1%	1%	3%	17%
ξ_θ [-]	μ	0.0096	0.0189	0.0309	0.0418	0.0148
	$\frac{\sigma}{\mu}$	3%	2%	2%	6%	12%

Table 5. Step 1.1a root mean square (RMS) of the vertical (z) and torsional displacement (z_{eq}): mean and standard deviation

		15 m/s	30 m/s	45 m/s	60 m/s	75 m/s
RMS z	μ	0.2603	0.778	1.3404	2.1601	4.4848
	$\frac{\sigma}{\mu}$	9%	6%	8%	5%	10%
RMS z_{eq}	μ	0.0419	0.2027	0.4792	0.9306	2.8414
	$\frac{\sigma}{\mu}$	25%	16%	12%	12%	7%

Table 6. Step 1.1a PSD of the vertical motion (reference values)

f [Hz]	15 m/s	30 m/s	45 m/s	60 m/s	75 m/s
0.001	0.12	1.19	5.60	23.86	147.27
0.010	0.12	1.15	5.40	22.46	124.42
0.100	4.09	20.58	34.35	44.54	53.18
0.278	0.00	0.00	0.02	0.03	0.05
0.300	0.00	0.00	0.01	0.02	0.03

Table 7. Step 1.1a PSD of the equivalent torsional motion (reference values)

f [Hz]	15 m/s	30 m/s	45 m/s	60 m/s	75 m/s
0.001	0.00	0.02	0.11	0.49	3.02
0.100	0.00	0.00	0.00	0.00	0.00
0.234	0.00	0.06	1.11	23.77	6.17
0.278	0.07	0.42	0.71	0.83	0.84
0.300	0.00	0.03	0.15	0.31	0.43

5 Conclusions

IABSE TG 3.1 concluded successfully the first part of its working plan, and results are presented in this paper. TG 3.1 group has a large and qualified participation and results represent the synthesis of many contributions. This aspect is very important, since one of the TG 3.1 goals is the definition of reference data for validation of numerical codes and usually these reference data cannot be obtained through closed-form analytical approaches due to the complexity of the modelling.

Reference data were therefore defined according to a statistical analysis of the results provided by TG 3.1 participants, considering the average of the available data, preliminarily depurated by outliers, and a confidence band defined according to the spread of the results.

Just for the buffeting response computation in Step 1.1a, where aerodynamic coefficients are analytically defined over the whole range of reduced velocity, as well as the incoming wind PSD, it is possible to analytically define the reference data. These analytical results are provided in the paper and compared to the statistical analysis of the results obtained by TG 3.1 participants, using different methods. The comparison highlights how the statistical post-processing of a wide and high-quality set of results allows for the definition of reliable reference data, supporting the adoption of this procedure in all the other benchmark steps.

To enhance the numerical codes validation, numerical results will be also compared against experimental results in Step 2 that is already in progress and whose results will be part of a future publication. Indeed, TG3.1 strategy to move with an increasing level of difficulty on the definition of numerical code validation turned out to be a correct procedure. In fact, even though Step 1.1a represents an oversimplified problem that considers only a sectional model with 2 DOFs and an analytically defined aerodynamics, results showed noticeable differences.

Concerning critical flutter velocities, the comparison showed a very limited spread of the results, once neglecting the outliers, but this parameter turned out to be not sufficient to validate the numerical methodology. Similar flutter speed values are obtained with completely different trends of aerodynamic damping vs wind speed, i.e. simulating a different aeroelastic behaviors.

The trend of the eigenvalues (frequency and damping) as functions of wind speed needs also to be analyzed together with the flutter wind speed for a correct evaluation of the numerical models.

A similar conclusion is also valid for RMS values in buffeting response, that can be obtained with very different PSD trends versus frequency. Again, in this case, the synthetic RMS value does not fully represent the quality of the aeroelastic modelling, but also PSD values should be compared to reference values.

Concerning the buffeting response computed in Step 1.1a with frequency domain approaches, it is surprising to find such a dispersion of results since the considered problem is intentionally oversimplified to limit the error source basically only to the numerical implementation of the methodologies.

Different is the case of time-domain approaches, where specific modelling of the aerodynamic forces, passing from frequency domain to time domain, is required and different methodologies are developed by the participants, justifying a larger dispersion as effectively shown in the results.

A following paper will show the already collected results of Step 1.1c where an additional level of

complexity is introduced by moving to real experimental aerodynamic coefficients and adding the lateral degree of freedom and the horizontal turbulent wind component.

6 Appendix

At a given wind speed U the equation of motion of the system is:

$$(-\omega^2[M_s + M_{se}(V^*)] + i\omega[R_s + R_{se}(V^*)] + [K_s + K_{se}(V^*)])X = F_{buff}(f) \quad (13)$$

where:

- $X = \begin{Bmatrix} Z \\ \Theta \end{Bmatrix}$ is the vector of free coordinates
- M_s, R_s, K_s are the structural mass, damping, and stiffness matrices
- M_{se}, R_{se}, K_{se} are the self-excited mass, damping, and stiffness matrices, written through flutter derivatives at a given reduced velocity V^*
- $F_{buff}(f)$ are the buffeting forces written through admittance functions at a given reduced velocity V^*
- $\omega = 2\pi f$ is the circular frequency;

The buffeting forces in frequency domain are defined through the Davenport function and the wind spectrum. Both are function of reduced velocity *V**, so at given wind speed U, they are function of the frequency f.

The power spectrum $S_w(f)$ is the PSD of the vertical component *w* of the wind velocity, defined through the Von Karman spectrum reported in Table 2. The Fourier transform of the vertical turbulent component $w(t)$ of the wind is $W_w(f)$. At a given wind speed U, the buffeting forces are defined in frequency domain as:

$$F_{buff}(f) = \frac{1}{2}\rho U B \begin{bmatrix} \chi_L(V^*) \\ B\,\chi_M(V^*) \end{bmatrix} W_w(f) \quad (14)$$

where:

- $\chi_L(V^*) = 2\pi\, A(V^*)$, and $A(V^*)$ is Davenport admittance function
- $\chi_M(V^*) = \frac{\pi}{2}\, A(V^*)$

For simplicity, buffeting forces in (16) can be written through a matrix $\chi_A(V^*)$ as:

$$F_{buff}(f) = \chi_A(V^*)\, W_w(f) \quad (15)$$

Considering the above buffeting forces as an input, the output of the system in frequency domain is:

$$X(f) = H(V^*)^{-1}\, F_{buff}(f) = H(V^*)^{-1}\chi_A(V^*)\, W_w(f) \quad (16)$$

where:

- $H(V^*) = (-\omega^2[M_s + M_{se}(V^*)] + i\omega[R_s + R_{se}(V^*)] + [K_s + K_{se}(V^*)])$ is the impedance matrix of the system at a given frequency f and reduced velocity V^*

Taking the complex conjugate transpose of the complex output vector X:

$$\overline{X(f)} = \overline{W_w(f)}\;\overline{\chi_A(V^*)}\;\overline{H(V^*)^{-1}} \quad (17)$$

The cross-spectrum matrix of the output X will be:

$$X\bar{X} = H(V^*)^{-1}\chi_A(V^*)W_w(f)\overline{W_w(f)}\;\overline{\chi_A(V^*)}\;\overline{H(V^*)^{-1}} \quad (18)$$

The cross-power spectrum matrix will be the expected value $E(X\bar{X})$ dividing by $2d_f$, where d_f is the frequency resolution:

$$S_X(f) = H(V^*)^{-1}\chi_A(V^*)S_w(f)\,\overline{\chi_A(V^*)}\;\overline{H(V^*)^{-1}} \quad (19)$$

where $S_X(f)$ is the cross-power spectrum matrix of the output, whose diagonal terms are the PSD of the vertical motion S_z and of the torsional motion S_θ.

A numerical example of the PSD computation is reported in order to help the validation procedure.

Selecting a wind velocity U of 45 m/s and a frequency f of 0.278 Hz (the structural torsional frequency), the reduced velocity $V^*$is equal to 5.22 and the PSD of the wind $S_w(f = 0.278)$ is 5.26 $\frac{\left(\frac{m}{s}\right)^2}{Hz}$.

The admittance matrix $\chi_A(V^* = 5.22)$ is:

$$\chi_A(V^* = 5.22\,) = \begin{bmatrix} 0.3584 \\ 2.7773 \end{bmatrix} 10^4$$

and the impedance matrix of the system at the given reduced velocity $V^*$is:

$$H(V^* = 5.22) = \begin{bmatrix} -0.0619 + 0.0056i & -0.1492 - 0.0811i \\ 0.0100 + 0.0419i & -1.1559 + 0.5382i \end{bmatrix} 10^6$$

The cross-power spectrum matrix of the output $S_X(f = 0.278)$, through Eq. (21) is:

$$S_X(f = 0.278) = \begin{bmatrix} 0.0167 & 0.0 - 0.007i \\ 0.0 + 0.007i & 0.0029 \end{bmatrix}$$

where the Power Spectrum Density of the vertical displacement is $S_z(f = 0.278) = 0.0167\ \frac{m^2}{Hz}$ and the Power Spectrum Density of the torsional displacement is $S_\theta(f = 0.278) = 0.0029\ \frac{rad^2}{Hz}$. The torsional values expressed in equivalent displacement of the deck leading edge according to: $S_{z_{eq}}(f) = \left(\frac{B}{2}\right)^2 S_\theta(f)$, is equal to $0.7062\ \frac{m^2}{Hz}$.

By repeating the example above for all the desired frequencies f and wind speeds V, it is possible to obtain the PSD reference curves in frequency domain, as shown in Figure 7 and in Figure 8 for a wind speed of 60 m/s.

References

[1] G. Diana, *Modelling of Vibrations of Overhead Line Conductors.,* Springer International Publishing, 2018.

[2] UIC518, *Testing and Approval of Railway Vehicles from the Point of View of Their Dynamic Behaviour: Safety, Track Fatigue, Ride Quality,* 2005.

[3] EN143636, *Testing and Simulation for the acceptance of running characteristics of railway vehicles - Running Behaviour and stationary tests,* 2016.

[4] EN50318, *Validation of simulation of the dynamic interaction between pantograph and overhead contact line,* 2002.

[5] C. Bucher e Y. Lin, «Stochastic stability of bridges considering coupled modes,» *Journal of Engineering Mechanics,* vol. 114(12), pp. 2055-2071, 1988.

[6] X. Chen, M. Matsumoto e A. Kareem, «Time domain flutter and buffeting response analysis of bridges,» *Journal of Engineering Mechanics,* vol. 126(1), pp. 7-16, 2000.

[7] I. Kavrakov e G. Morgenthal, «A comparative assessment of aerodynamic models for buffeting and flutter of long-span bridges,» *Engineering,* vol. 3, pp. 823-838, 2017.

[8] I. Garrick, *On some reciprocal relations in the theory of nonstationary flows,* NACA, 1938.

[9] A. Jain, N. Jones e R. Scanlan, «Coupled Flutter and Buffeting Analysis of Long-Span Bridges,» *Journal of Structural Engineering.,* vol. 122(7), pp. 716-725, 1996.

[10] O. Oiseth e R. Sigbjörnsson, «An alternative analytical approach to prediction of flutter stability limits of cable supported bridges,» *Journal of Sound and Vibration.,* vol. 330(12), pp. 2784-2800, 2011.

[11] O. Oiseth, A. Ronnquist e R. Sigbjörnsson, «Finite element formulation of the self-excited forces for time-domain assessment of wind-induced dynamic response and flutter stability limit of cable-supported bridges.,» *Finite Elements in Analysis and Design,* vol. 50, pp. 173-183, 2012.

[12] O. Oiseth, A. Ronnquist e R. Sigbjörnsson, «Simplified prediction of wind-induced response and stability limit of slender long-span suspension bridges based on modified quasi-steady theory: A case study.,» *Journal of Wind Engineering and Industrial Aerodynamics,* vol. 98(12), pp. 730-741, 2010.

[13] O. Oiseth, A. Ronnquist and R. Sigbjörnsson, "Time domain modeling of self-excited aerodynamic forces for cable-supported bridges: A comparative study," *Computers & Structures,* Vols. 89(13-14), pp. 1306-1322, 2011.

[14] M. Shinozuka, «Monte Carlo solution of structural dynamics,» *Computers and*

Structures, Vol. %1 di %22(5-6), pp. 855-874, 1972.

[15] M. Shinozuka e C. Jan, «Digital simulation of random processes and its applications,» *Journal of Sound and Vibration,* vol. 25(1), pp. 111-128, 1972.

[16] S. Stoyanoff, «A unified approach for 3D stability and time domain response analysis with application of quasi steady theory,» *Journal of Wind Engineering and Industrial Aerodynamics,* vol. 89, p. 1591–1606, 2001.

[17] S. Stoyanoff, *Wind Induced Vibrations of Cable-Stayed Bridges,* Kyoto University, Japan, , 1993.

[18] S. Stoyanoff e P. Dallaire, «A direct method for calculation of wind loads on long- span bridges,» in *12th Americas Conference on Wind Engineering (12ACWE)*, Seattle, Washington, USA, 2013.

[19] J. Park, K. Jung, Y. Hong, H. Kim e H. Lee, «Exact Enforcement of the Causality Condition on the Aerodynamic Impulse Response Function Using a Truncated Fourier Series,» *Journal of Engineering Mechanics,* vol. 140(5), 2014.

[20] K. Jung, H. Kim e H. Lee, «Evaluation of impulse response functions for convolution integrals of aerodynamic forces by optimization with a penalty function,» *Journal of Engineering Mechanics,* vol. 138(5), pp. 519-529, 2011.

[21] K. Jung, H. Kim e H. Lee, «New Unified Approach for Aeroelastic Analyses Using Approximate Transfer Functions of Aerodynamic Forces,» *Journal of Engineering Mechanics,* vol. 140(4), 2013.

[22] E. N. Strømmen, Theory of Bridge Aerodynamics, Springer, 2010.

[23] M. Matsumoto, K. Okubo, Y. Ito, H. Matsumiya e G. Kim, «The complex branch characteristics of coupled flutter,» *Journal of Wind Engineering and Industrial Aerodynamics,* vol. 96(10), pp. 1843-1855, 2011.

[24] J. Høgsberg, J. Krabbenhøft e S. Krenk, «State space representation of bridge deck aeroelasticity,» in *13th Nordic Seminar on Computational Mechanics*, Oslo, Norway, 2000.

[25] T. Argentini, A. Pagani, D. Rocchi e A. Zasso, «Monte Carlo analysis of total damping and flutter speed of a long span bridge: Effects of structural and aerodynamic uncertainties,» *Journal of Wind Engineering and Industrial Aerodynamics,* vol. 128, pp. 90-10, 2014.

[26] G. Diana, D. Rocchi e T. Argentini, «An experimental validation of a band superposition model of the aerodynamic forces acting on multi-box deck sections,» *Journal of Wind Engineering & Industrial Aerodynamics,* vol. 113, pp. 40-58, 2013.

[27] G. Diana, D. Rocchi e T. Argentini, «Buffeting response of long span bridges: numerical-experimental validation of fluid-structure interaction models,» in *IABSE Conference - Structural Engineering: Providing Solutions to Global Challenges*, Geneva, 2015.

[28] Q. Ding, L. Zhu e H. Xiang, «Simulation of stationary Gaussian stochastic wind velocity field. Wind and Structures,» *An International Journal,* vol. 9, pp. 231-243, 2006.

[29] G. Deodatis, «Simulation of ergodic multivariate stochastic processes,» *Journal of Engineering Mechanics,* vol. 122, pp. 778-787, 1996.

[30] G. Diana, F. Resta, A. Zasso, M. Belloli e D. Rocchi, «Forced motion and free motion aeroelastic tests on a new concept dynamometric section model of the Messina

suspension bridge,,» *Journal of Wind Engineering and Industrial Aerodynamics,* vol. 92, pp. 441-462, 2004.

[31] H. Dewey Hodges e G. Alvin Pierce, Introduction to Structural Dynamics and Aeroelasticity, Cambridge University Press, 2012.